



Article

# A Molecular Dynamics Study of the Stability and Mechanical Properties of a Nano-Engineered Fuzzy Carbon Fiber Composite

Hassan Almousa<sup>1,2</sup>, Qing Peng<sup>1,3,4</sup>  and Abduljabar Q. Alsayoud<sup>4,5,\*</sup> 

<sup>1</sup> Physics Department, King Fahd University of Petroleum & Minerals, Dhahran 31261, Saudi Arabia; hassan.almousa@aramco.com (H.A.); qing.peng@kfupm.edu.sa (Q.P.)

<sup>2</sup> Research & Development Center, Saudi Aramco, Dhahran 31311, Saudi Arabia

<sup>3</sup> KACARE Energy Research & Innovation Center at Dhahran, Dhahran 31261, Saudi Arabia

<sup>4</sup> Hydrogen Energy and Storage Center, King Fahd University of Petroleum & Minerals, Dhahran 31261, Saudi Arabia

<sup>5</sup> Material Science and Engineering Department, King Fahd University of Petroleum & Minerals, Dhahran 31261, Saudi Arabia

\* Correspondence: sayoudaq@kfupm.edu.sa

**Abstract:** Carbon fiber-reinforced polymer composites are used in various applications, and the interface of fibers and polymer is critical to the composites' structural properties. We have investigated the impact of introducing different carbon nanotube loadings to the surfaces of carbon fibers and characterized the interfacial properties by molecular dynamics simulations. The carbon fiber (CF) surface structure was explicitly modeled to replicate the graphite crystallites' interior consisting of turbostratic interconnected graphene multilayers. Then, single-walled carbon nanotubes and polypropylene chains were packed with the modeled CFs to construct a nano-engineered "fuzzy" CF composite. The mechanical properties of the CF models were calculated through uniaxial tensile simulations. Finally, the strength to peel the polypropylene from the nano-engineered CFs and interfacial energy were calculated. The interfacial strength and energy results indicate that a higher concentration of single-walled carbon nanotubes improves the interfacial properties.

**Keywords:** fuzzy carbon fiber; turbostratic interconnected graphene; molecular dynamics; interfacial property; uniaxial deformation



**Citation:** Almousa, H.; Peng, Q.; Alsayoud, A.Q. A Molecular Dynamics Study of the Stability and Mechanical Properties of a Nano-Engineered Fuzzy Carbon Fiber Composite. *J. Compos. Sci.* **2022**, *6*, 54. <https://doi.org/10.3390/jcs6020054>

Academic Editors: Jiadeng Zhu, Gouqing Li and Lixing Kang

Received: 10 January 2022

Accepted: 2 February 2022

Published: 10 February 2022

**Publisher's Note:** MDPI stays neutral with regard to jurisdictional claims in published maps and institutional affiliations.



**Copyright:** © 2022 by the authors. Licensee MDPI, Basel, Switzerland. This article is an open access article distributed under the terms and conditions of the Creative Commons Attribution (CC BY) license (<https://creativecommons.org/licenses/by/4.0/>).

## 1. Introduction

Greenhouse gases trap heat in the atmosphere, increasing Earth's surface temperature from 1–4 °C by 2100 [1]. One of the significant contributors to emitting these gases is the transportation sector [2]. Energy consumption in transport is dependent on a vehicle's mass. Therefore, reducing the vehicle's weight will have an immediate positive impact on reducing the emitted gases. A study showed that reducing the weight of a passenger car by 27% can reduce its emissions by 40% [3]. New materials with low density and high strength need to be utilized to replace conventional metals for weight reduction, and carbon fiber-reinforced polymer (CFRP) composites are the most fitting candidate for this job. Carbon fibers (CFs) have high strength, high modulus, and low density [4]. These outstanding properties have made them essential as reinforcement in structural materials for many areas, such as aerospace, automotive, high-grade sports, and many other applications [5]. However, under compression, fiber-reinforced composites suffer a range of failures typically associated with fiber micro-buckling or kinking linked to the interfacial issues. Additionally, the anisotropic nature of composite materials and their internal interface tend to drive the accumulation of internal damage and result in a possible catastrophic failure [6].

A conventional solution is the dispersion of additives such as carbon nanotubes (CNTs) in a polymer matrix. Computational studies indicated improvement in the elastic-plastic

response, fracture toughness, and fiber/matrix stiffness by altering the load path under debonding. However, local agglomeration of CNTs causes microscopic stress concentrations that induce premature damage [7,8]. Therefore, new constituents and processes became available to create nano-engineered interphases of CNTs on the CF surface. This concept has been experimentally demonstrated using a chemical vapor deposition process and electro-deposition methods for linking CNTs to CF surfaces via van der Waals interaction [9,10]. The so-called “fuzzy” CFs contain a microfiber core made of carbon coated with CNTs prior to matrix impregnation. The fuzzy fiber is hierarchical and shows enhanced fracture toughness, interlaminar shear strength, and thermal and electrical properties [11]. To further understand this type of hierarchical fiber and its potential without the challenging experimental parametrization, an atomistic model framework was constructed for investigating the interface interaction between the fuzzy CF and the polymer matrix.

Molecular dynamics (MD) simulation is a well-established and reliable atomistic model for various applications [12–14]. A series of MD simulations were conducted first to construct the following components individually: CFs, single-walled carbon nanotubes (SWCNTs), and polypropylene (PP) as the matrix. This model was then subjected to uniaxial stress deformation through MD simulation. In MD simulations, materials are a combination of atoms that are regarded as classical mass particles. This technique is based on tracking the trajectories of atoms in a modeled system that can provide data with the time evolution of a nanostructured material subjected to external conditions. Ultimately, the computation involves position, velocity, and acceleration as a solution to Newton’s second law [15]. Additionally, force fields are used to describe the interatomic interactions. The selection of an appropriate force field is critical for the validity of MD simulations. Therefore, several force fields have been developed for different material systems [16–19]. Subsequently, the motivation of this study is to demonstrate efficiently, via MD computational methods, the significance of nano-engineering CF surfaces with CNTs in thermoplastic-based composites as a valuable lightweight structure for transportation applications.

## 2. Methods

### 2.1. Model

To model the complex nano-engineered fuzzy CFs embedded in the polymer matrix, subsequent simulation steps were required to construct the system and then perform mechanical and interfacial analysis. The CF microstructure has interior graphite crystallites consisting of turbostratic interconnected graphene multilayers. Several atomistic approaches and computational tools were used to generate 2D and 3D microstructures of CF. The simulations range from surface studies with simplified graphene layers [20–22] and graphite blocks annealing [23] to complex precursor and reactive simulations [24,25] for the analysis of CF chemistry and mechanical properties. Therefore, an MD simulation (See Section 2.2.1) was used to model the range of CF microstructures with varied degrees of graphitic region. The thermoplastic PP chain of 40 monomers with an atactic configuration was built through the Polymer Modeler tool [26]. In addition, an (8,6) SWCNT with a length of 2.5 nm and a diameter of 0.95 nm was built by the Visual Molecular Dynamics (VMD) extension of the nanobuilder tool [27]. The experimental diameter and length of nanotubes grown on a CF surface are typically about 10 nm and 125 nm, respectively [28]. Nonetheless, the interaction energy decreases as the nanotube diameter increases [29]. For the following study, the chosen dimensions are sufficient to investigate the interfacial properties. After building the above constituents, the CFs were modified by introducing both CNTs on the surface and including 20 PP chains through the PACKMOL software package [30]. A tolerance level of 2.0 Å was selected to perform the PACKMOL packing through several iterations to find the optimum configuration. Additionally, the  $x$ - and  $y$ -axis dimensions were set based on the built CF models as the center of mass. Moreover, the SWCNT was varied in loading percentages as 0, 1, and 3 wt% based on the assumption that the model was a 60 wt% and 40 wt% of matrix and fibers, respectively. Finally, the

nano-engineered CF composites were visualized by the Open Visualization Tool (OVITO) software [31], as shown in Figure 1.

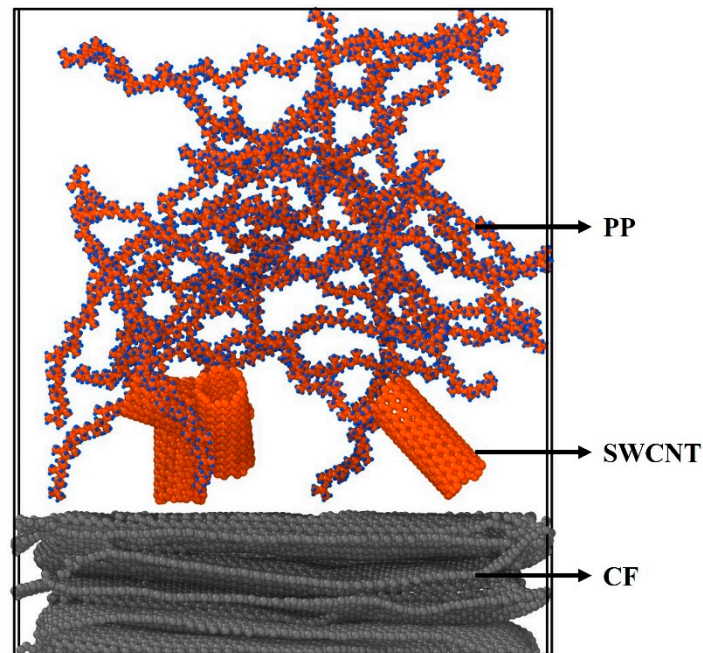


**Figure 1.** Nano-engineered carbon fiber composite model built with PACKMOL consisting of carbon fibers and turbostratic interconnected graphene multilayered structure with a density of  $1.69 \text{ g/cm}^3$  coated with four (8, 6) 2.5 nm in length and 0.95 nm in diameter single-walled carbon nanotubes entangled with twenty atactic 40-monomer polypropylene chains.

## 2.2. Molecular Dynamic Simulations

The MD simulations were conducted using a large-scale atomic/molecular massively parallel simulator (LAMMPS) [32]. Through time and ensemble average of motion trajectory, the dynamic properties of the system were obtained. It can model extensive systems using a variety of interatomic potentials and boundary conditions. For CF model simulation, Tersoff empirical interatomic potential described the total binding energy. This potential incorporates a dependency on the number of bonds between a pair of atoms. The general form of the Tersoff formula is given in Equation (1), where  $i j$  indicates the interacting atoms,  $B_{ij}$  is the bond order between  $i$  and  $j$ , and  $\varnothing_R$  and  $\varnothing_A$  are the repulsive and attractive potentials, respectively [33]. The remaining simulations have been conducted with the modified potential AIREBO-m. It replaces the singular Lennard–Jones potential with a Morse potential, compared to the original AIREBO potential. The Morse potential is presented in Equation (2), where  $\alpha$  is a curvature modification parameter, and  $\epsilon$  and  $r^{eq}$  correspond to the minimum energy depth and location, respectively [34]. Researchers have modified the cutoff distances based on specified system studies to adopt this potential for large deformation. This modification was mainly applied to count for the tilt grain boundaries effect on the strength of graphene [35–37]. In this paper, an  $r_{cc}^{\min}$  parameter of the value of  $1.92 \text{ \AA}$  was adopted based on previous work done on deformation of graphene structures [13,14].

$$\varnothing_{ij}(r_{ij}) = [\varnothing_R(r_{ij}) - B_{ij}\varnothing_A(r_{ij})] \quad (1)$$

$$U_{ij}(r) = -\epsilon_{ij} \left[ 1 - \left( 1 - e^{-\alpha_{ij}(r-r_{ij}^{eq})} \right)^2 \right] \quad (2)$$

### 2.2.1. Carbon Fiber Simulation

The inspiration for CF models was taken from Zhu et al.'s work [38]. The concept is to stack several graphene layers and anneal them at high temperatures to disturb the crystalline structure and create turbostratic interconnected graphene multilayers that define a CF microstructure. A  $(56.3 \times 109.6 \times 28.0) \text{ \AA}^3$  simulation box consisting of eight graphene layers with 15,739 or 16,120 carbon atoms to vary the final densities was built. The system was first equilibrated at a temperature of 300 K in 10 ps using a Nose–Hoover thermostat [39] with periodic boundary conditions in a canonical ensemble (NVT). Next, the temperature was ramped to 3500–5500 K at a rate of 110 K/ps, followed by relaxation for 60 ps at the same temperature. Afterward, extremely rapid quenching of 2750 K/ps to a temperature of 300 K was performed to preserve the turbostratic arrangements and graphene regions. Finally, the system was fully relaxed in an isothermal-isobaric ensemble (NPT) for 10 ps at a temperature of 300 K to release any internal stresses. The simulation process is summarized in Figure 2 with illustrations of the structure evolution throughout the process in a polyhedral template matching to show the graphene regions and regular visualization via OVITO.

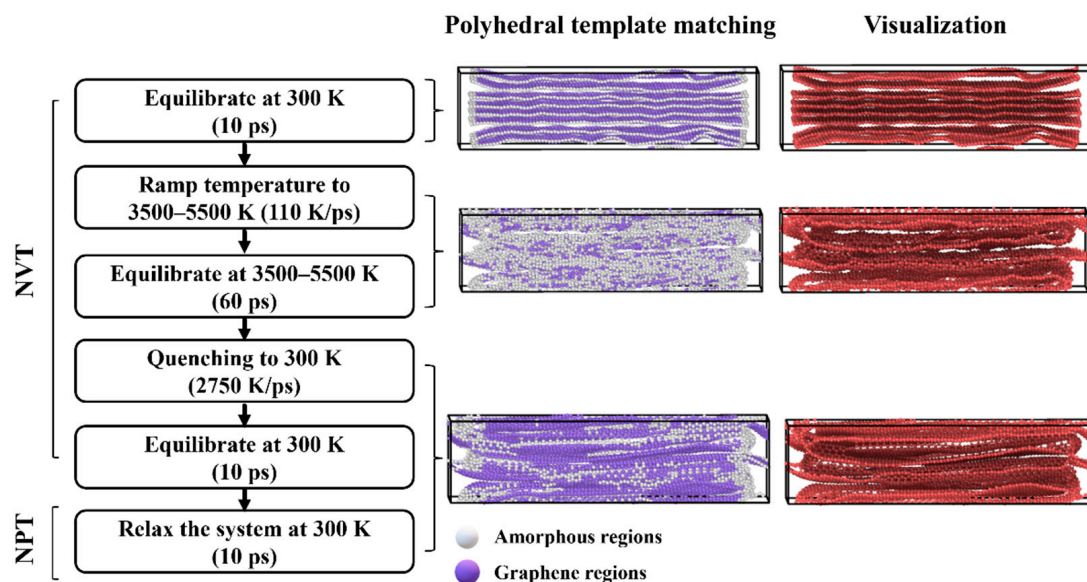


**Figure 2.** Molecular dynamic simulation steps for building a carbon fiber structure via annealing methodology using the NVT and NPT ensembles with different graphene regions percentages and turbostratic arrangements. Polyhedral template matching represents the amorphous regions in white and the graphene regions in purple.

### 2.2.2. Uniaxial Stress Simulation

Atomistic simulation of uniaxial tensile loading can be conducted with a parallel molecular dynamics code. After equilibrating any of the developed structures, the simulation box was deformed in the targeted direction at a strain rate of 0.001/ps. First, MD deformation in the long direction with periodic boundary conditions in all directions was conducted to analyze the strength of the developed CF models. The simulation was conducted at a temperature of 300 K using the Nose–Hoover thermostat and the AIREBO-m potential. Second, the interfacial analysis for the nano-engineered CF composite system was conducted by deformation in the z-direction with a fixed boundary and periodic boundary condition in the x- and y-directions, respectively. Moreover, the simulation was conducted at 50 K after an equilibration time of 20 ps using the AIREBO-m potential. Then, uniaxial stress of 15% strain was applied in the z-axis to peel the PP from the nano-engineered CF surface for theoretical strength and interfacial energy calculations.

### 3. Results and Discussions

#### 3.1. Carbon Fiber Model Properties

After completing the CF microstructure simulation, four different models (Table 1) were developed by varying the number of carbon atoms and the maximum temperature. This resulted in densities close to the density of real CFs and graphene region percentages. All the developed models showed clear stress-strain curves (Figure 3), with a range of strength and Young's modulus caused by the differences in densities and graphene region percentages. The simulated strength values ranged from 9.9 to 26.7 GPa and Young's modulus of 129.6 to 277 GPa. In comparison, the experimental values of carbon fiber strength and Young's modulus are 3.0–7.0 GPa and 200–450 GPa, respectively [4,40]. The computational tensile strength values were higher than the experimental values because of the absence of defects inside the components, the extremely high loading rate, and length-scale discrepancies. The simulated microstructures were around three orders of magnitude smaller than the experimental samples, and thus the maximum simulated pore size is small compared to the experimental. The larger pores in experimental samples act as stress concentration sites and thus lead to brittle fracture and lower strength. Moreover, the published work of computational large-scale carbon fiber microstructure stress-strain curves by Zhu et al. [25] for three different structures have resulted in a comparable range of strength values between 6.73–6.90 GPa and Young's modulus of 95.9–284.5 GPa. Last, the simulated CF models showed crystallite arrangement around the longitudinal axis with turbostratic stacks of graphite structure, as shown in Figures S6–S9. This structure was reported for physical CF via X-ray diffraction and TEM images [41,42].

**Table 1.** The resulting physical and mechanical properties of the used carbon fiber models.

Model	Annealing Temperature (K)	Number of Carbon Atoms	Density (g/cm <sup>3</sup> )	Graphene Region (%)	Strength (GPa)	Young's Modulus (GPa)
B1	5500	15,739	1.64	70	9.9	138.1
B2	4500	15,739	1.63	71	10.5	129.6
B3	3500	16,120	1.68	84	26.7	277.0
B4	4500	16,120	1.69	85	24.6	261.0

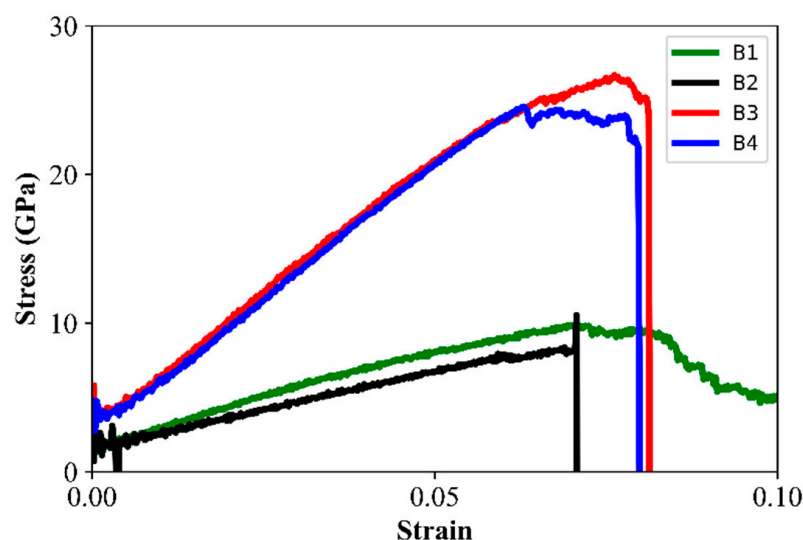


**Figure 3.** Stress-strain curves predicted in axial deformation of simulated carbon fiber structures with a maximum value of Young's modulus equal to 277.0 GPa and tensile strength of 26.7 GPa for the B3 model.

### 3.2. Nano-Engineered CF Composites Interfacial Properties

The four developed CF models were transformed into nano-engineered composites by introducing SWCNTs and PP via PACKMOL. The result was the construction of 12 different structures, with each CF model loaded with 0, 1, and 3 wt% SWCNTs. The calculations were conducted for the complex structures with the theoretical assumptions of low-temperature deformation after equilibration. However, the SWCNTs' positions can represent a minimized arrangement as local minimum energy and not the global minimum energy. Nonetheless, the non-bonding van der Waals (vdW) interactions were the main interactions that governed the three different constitutes, and among the PP chains, SWCNTs, and graphene layers. The calculated interfacial strength of each CF model was the stress required to peel PP chains away from the nano-engineered CFs, plotted against the averaged loading percentages of SWCNTs, as shown in Figure 4. The required strength increased linearly with the addition of SWCNTs in comparison to the pristine CFs, and independently from the CF model. The enhancement of interfacial strength resulted in an improved load transfer to the CFs [43]. This observation can be attributed to the increase in non-bonded vdW interactions, as the PP chains can entangle and interact with a larger carbon surface area. Moreover, mechanical interlocking can also contribute to the increase in strength. Experimentally, S. Yumitori et al. [44] showed that the interfacial shear strength improved by 35% in a CF/PP composite after grafting CFs with CNTs by performing a fiber pull-out test.

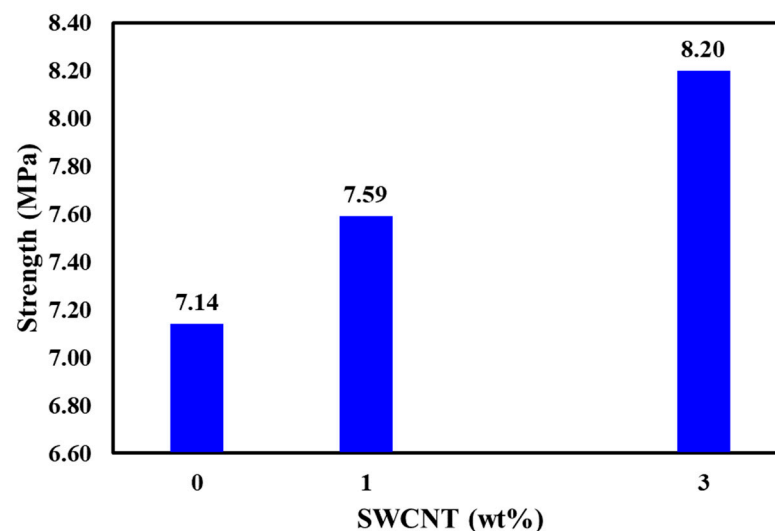


**Figure 4.** Average value of peeling strength to separate polypropylene from nano-engineered carbon fibers for the four developed CF structures with different loading percentages of 0, 1, and 3 wt% for single-walled carbon nanotubes after a 15% strain in the z-direction.

Potential energy is a function of several components, such as torsion, Lennard–Jones (LJ), pair, and REBO energies. Therefore, the calculated interfacial energy is the delta between the total potential energy and other components. Figure 5 shows the interfacial energy and other components as a function of displacement of the nano-engineered CFs from PP chains in the z-direction. This indicates that the dominant interfacial energy response to the complex model was based strictly on the non-bonded vdW interactions between the PP chains and the nano-engineered CFs. As a result, the interfacial energy increased linearly and reached a plateau trend. The same behavior was reported previously on SWCNT interaction with polyethylene (PE) chains [45].

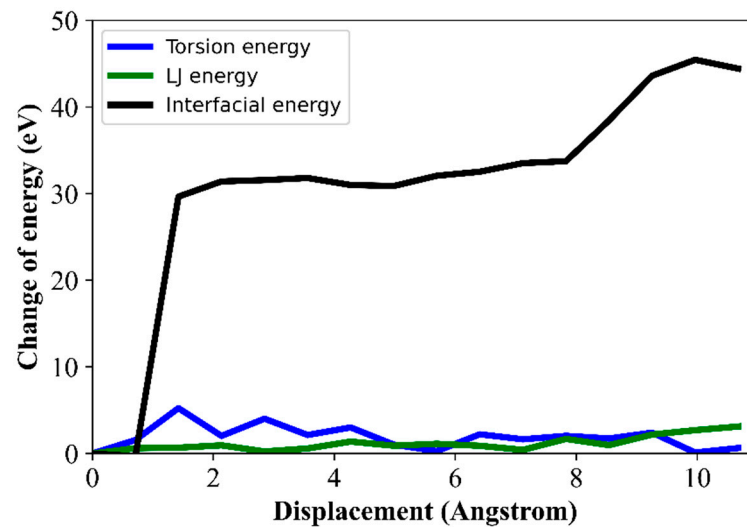


**Figure 5.** Change of the potential energy as a function of the displacement of nano-engineered carbon fiber-B4 with 3 wt% (8,6) 2.5 nm in length and 0.95 nm in diameter single-walled carbon nanotubes from twenty atactic 40-monomer polypropylene chains in the z-direction.

Accordingly, the interfacial energy of different SWCNT loadings was averaged and plotted in Figure 6. The models with 3 wt% loading showed a significant increase in the interfacial energy because of the increase in the non-bonded vdW interactions. Below the two angstroms mark, the interfacial energy peaked, and energy values increased with the SWCNTs' higher loadings. This observation indicates an improvement in the interfacial properties of nano-engineered CFs compared to pristine CFs.

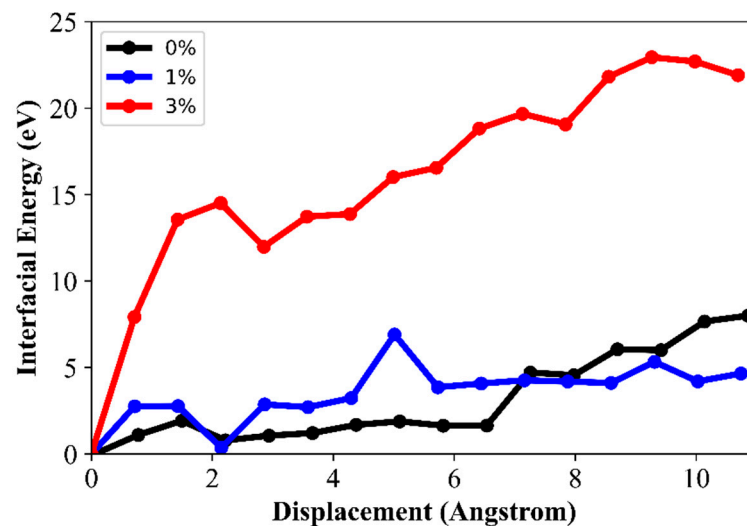


**Figure 6.** Averaged interfacial energy of four models of nano-engineered carbon fibers for each single-walled carbon nanotube loading percentage as a function of displacement in the z-direction from the twenty atactic 40-monomer polypropylene chains.

#### 4. Conclusions

We have assessed the interfacial properties of nano-engineered CF composites using MD simulations. Four different CF models were developed with graphene sheets and an annealing process governed by Tersoff potential to produce models with a density range of 1.63–1.69 g/cm<sup>3</sup>, and graphene region percentage ranging from 70–85%. The built CF structures showed the turbostratic interconnected graphene multilayer arrangement with strengths ranging from 9.9–26.7 GPa and Young's modulus of 129.6–277.0 GPa. The tensile

strength values of the CFs were higher than the experimental because of the high loading rate and length-scale discrepancy.

Moreover, a nano-engineered CFRP was constructed with PP and SWCNTs using PACKMOL. The interfacial energy just below two angstroms increased by 180% and 700% for the 1 and 3 wt% SWCNT loading, respectively. The stress required to peel PP from the nano-engineered CFs also showed an increasing trend due to the enhancement in non-bonded vdW interactions. Finally, the nano-engineered CFRP is considered to be a multi-functional composite that can serve beyond structural applications [11]. This advancement in structural components for the automotive industry can contribute to emissions reduction. Therefore, the explored theoretical atomistic modeling in this paper may lay a building block for more advanced computational research to design and optimize nano-engineered CFs.

**Supplementary Materials:** The following supporting information can be downloaded at: <https://www.mdpi.com/article/10.3390/jcs6020054/s1>.

**Author Contributions:** H.A., A.Q.A. and Q.P. contributed conception and design of the study. H.A. performed the calculations. H.A., A.Q.A. and Q.P. performed the statistical analysis. H.A. wrote the first draft of the manuscript. All authors have read and agreed to the published version of the manuscript.

**Funding:** Q. P. would like to acknowledge the support provided by the Deanship of Scientific Research (DSR) at King Fahd University of Petroleum & Minerals (KFUPM) through the K.A.CARE project (KACARE211-RFP-02). For computer time, this research used the resources of the Supercomputing Laboratory at King Abdullah University of Science Technology (KAUST) in Thuwal, Saudi Arabia, through project #1532.

**Data Availability Statement:** The datasets generated and/or analyzed during the current study are available from the corresponding author on reasonable request.

**Acknowledgments:** We would like to thank Hassan Shoab and Jafar Albinmoussa for the useful discussions.

**Conflicts of Interest:** There are no conflicts of interest to declare.

## References

1. Aizebeokhai, A.P. Global Warming and Climate Change: Realities, Uncertainties and Measures. *Int. J. Phys. Sci* **2009**, *4*, 868–879. [[CrossRef](#)]
2. Albuquerque, F.D.B.; Maraqa, M.A.; Chowdhury, R.; Mauga, T.; Alzard, M. Greenhouse Gas Emissions Associated with Road Transport Projects: Current Status, Benchmarking, and Assessment Tools. In *Transportation Research Procedia*; Elsevier B.V.: Amsterdam, The Netherlands, 2020; Volume 48, pp. 2018–2030. [[CrossRef](#)]
3. Windisch, E.; Benezech, V.; Chen, G.; Kauppila, J. *Lightening Up: How Less Heavy Vehicles Can Help Cut CO<sub>2</sub> Emissions*; OECD: Paris, France, 2017.
4. Newcomb, B.A. Processing, Structure, and Properties of Carbon Fibers. *Compos. Part A* **2016**, *91*, 262–282. [[CrossRef](#)]
5. Das, T.K.; Ghosh, P.; Das, N.C. Preparation, Development, Outcomes, and Application Versatility of Carbon Fiber-Based Polymer Composites: A Review. *Adv. Compos. Hybrid Mater.* **2019**, *2*, 214–233. [[CrossRef](#)]
6. Kyriakides, S.; Arseculeratne, R.; Perry, E.J.; Liechti, K.M. On the compressive failure of fiber reinforced composites. *Int. J. Solids Structures* **1995**, *32*, 689–738. [[CrossRef](#)]
7. Imani Yengejeh, S.; Kazemi, S.A.; Öchsner, A. Carbon Nanotubes as Reinforcement in Composites: A Review of the Analytical, Numerical and Experimental Approaches. *Comput. Mater. Sci.* **2017**, *136*, 85–101. [[CrossRef](#)]
8. Clancy, A.J.; Anthony, D.B.; de Luca, F. Metal Mimics: Lightweight, Strong, and Tough Nanocomposites and Nanomaterial Assemblies. *ACS Appl. Mater. Interfaces* **2020**, *12*, 15955–15975. [[CrossRef](#)]
9. Zhao, J.; Liu, L.; Guo, Q.; Shi, J.; Zhai, G.; Song, J.; Liu, Z. Growth of Carbon Nanotubes on the Surface of Carbon Fibers. *Carbon* **2008**, *46*, 380–383. [[CrossRef](#)]
10. Bekyarova, E.; Thostenson, E.T.; Yu, A.; Kim, H.; Gao, J.; Tang, J.; Hahn, H.T.; Chou, T.W.; Itkis, M.E.; Haddon, R.C. Multiscale Carbon Nanotube-Carbon Fiber Reinforcement for Advanced Epoxy Composites. *Langmuir* **2007**, *23*, 3970–3974. [[CrossRef](#)]
11. Qian, H.; Greenhalgh, E.S.; Shaffer, M.S.P.; Bismarck, A. Carbon Nanotube-Based Hierarchical Composites: A Review. *J. Mater. Chem.* **2010**, *20*, 4751–4762. [[CrossRef](#)]
12. Peng, Q.; Meng, F.; Yang, Y.; Lu, C.; Deng, H.; Wang, L.; De, S.; Gao, F. Shockwave Generates <100> Dislocation Loops in Bcc Iron. *Nat. Commun.* **2018**, *9*, 4880. [[CrossRef](#)]

13. Deng, B.; Hou, J.; Zhu, H.; Liu, S.; Liu, E.; Shi, Y.; Peng, Q. The Normal-Auxeticity Mechanical Phase Transition in Graphene. *2D Materials* **2017**, *4*, 021020. [CrossRef]
14. Hou, J.; Deng, B.; Zhu, H.; Lan, Y.; Shi, Y.; De, S.; Liu, L.; Chakraborty, P.; Gao, F.; Peng, Q. Magic Auxeticity Angle of Graphene. *Carbon* **2019**, *149*, 350–354. [CrossRef]
15. Rapaport, D.C. *The Art of Molecular Dynamics Simulation*, 2nd ed.; Cambridge University Press: Cambridge, UK, 2004.
16. Ritschl, F.; Fait, M.; Fiedler, K.; Khler, J.E.H.; Kubias, B.; Meisel, M. An Extension of the Consistent Valence Force Field (CVFF) with the Aim to Simulate the Structures of Vanadium Phosphorus Oxides and the Adsorption of n-Butane and of 1-Butene on Their Crystal Planes. *Z. Anorg. Allg. Chem.* **2002**, *628*, 1385–1396. [CrossRef]
17. Sun, H. Ab Initio Calculations and Force Field Development for Computer Simulation of Polysilanes. *Macromolecules* **1995**, *28*, 701–712. [CrossRef]
18. Sun, H. Compass: An Ab Initio Force-Field Optimized for Condensed-Phase Applications—Overview with Details on Alkane and Benzene Compounds. *J. Phys. Chem. B* **1998**, *102*, 7338–7364. [CrossRef]
19. Van Duin, A.C.T.; Dasgupta, S.; Lorant, F.; Goddard, W.A. ReaxFF: A Reactive Force Field for Hydrocarbons. *J. Phys. Chem. A* **2001**, *105*, 9396–9409. [CrossRef]
20. Allington, R.D.; Attwood, D.; Hamerton, I.; Hay, J.N.; Howlin, B.J. A Model of the Surface of Oxidatively Treated Carbon Fibre Based on Calculations of Adsorption Interactions with Small Molecules. *Compos. Part A* **1998**, *29*, 1283–1290. [CrossRef]
21. Allington, R.D.; Attwood, D.; Hamerton, I.; Hay, J.N.; Howlin, B.J. Developing Improved Models of Oxidatively Treated Carbon Fibre Surfaces, Using Molecular Simulation. *Compos. Part A* **2004**, *35*, 1161–1173. [CrossRef]
22. Awan, I.S.; Xiaoqun, W.; Pengcheng, H.; Shanyi, D. Developing an Approach to Calculate Carbon Fiber Surface Energy Using Molecular Simulation and Its Application to Real Carbon Fibers. *J. Compos. Mater.* **2012**, *46*, 707–715. [CrossRef]
23. Penev, E.S.; Artyukhov, V.I.; Jakobson, B.I. Basic Structural Units in Carbon Fibers: Atomistic Models and Tensile Behavior. *Carbon* **2015**, *85*, 72–78. [CrossRef]
24. Rajabpour, S.; Mao, Q.; Gao, Z.; Khajeh Talkhonch, M.; Zhu, J.; Schwab, Y.; Kowalik, M.; Li, X.; van Duin, A.C.T. Low-Temperature Carbonization of Polyacrylonitrile/Graphene Carbon Fibers: A Combined ReaxFF Molecular Dynamics and Experimental Study. *Carbon* **2021**, *174*, 345–356. [CrossRef]
25. Zhu, J.; Gao, Z.; Kowalik, M.; Joshi, K.; Ashraf, C.M.; Arefev, M.I.; Schwab, Y.; Bumgardner, C.; Brown, K.; Burden, D.E.; et al. Unveiling Carbon Ring Structure Formation Mechanisms in Polyacrylonitrile-Derived Carbon Fibers. *ACS Appl. Mater. Interfaces* **2019**, *11*, 42288–42297. [CrossRef] [PubMed]
26. Haley, B.; Wilson, N.; Li, C.; Arguelles, A.; Jaramillo, E.; Strachan, A. Polymer Modeler. 2010. Available online: <https://nanohub.org/resources/polymod> (accessed on 14 June 2021).
27. Humphrey, W.; Dalke, A.; Schulten, K. VMD—Visual Molecular Dynamics. *J. Molec. Graphics* **1996**, *14*, 33–38. [CrossRef]
28. Anthony, D.B.; Sui, X.M.; Kellersztein, I.; de Luca, H.G.; White, E.R.; Wagner, H.D.; Greenhalgh, E.S.; Bismarck, A.; Shaffer, M.S.P. Continuous Carbon Nanotube Synthesis on Charged Carbon Fibers. *Compos. Part A* **2018**, *112*, 525–538. [CrossRef]
29. Rouhi, S.; Alizadeh, Y.; Ansari, R. Molecular Dynamics Simulations of the Interfacial Characteristics of Polypropylene/Single-Walled Carbon Nanotubes. *Proc. IMechE Part L J. Mater. Des. Appl.* **2016**, *230*, 190–205. [CrossRef]
30. Martinez, L.; Andrade, R.; Birgin, E.G.; Martínez, J.M. PACKMOL: A Package for Building Initial Configurations for Molecular Dynamics Simulations. *J. Comput. Chem.* **2009**, *30*, 2157–2164. [CrossRef]
31. Stukowski, A. Visualization and Analysis of Atomistic Simulation Data with OVITO—the Open Visualization Tool. *Modelling Simul. Mater. Sci. Eng.* **2010**, *18*, 015012. [CrossRef]
32. Plimpton, S. Fast Parallel Algorithms for Short-Range Molecular Dynamics. *J. Comput. Phys.* **1995**, *117*, 1–19. [CrossRef]
33. Tersoff, J. Empirical Interatomic Potential for Carbon, with Applications to Amorphous Carbon. *Phys. Rev. Lett.* **1988**, *61*, 2879–2882. [CrossRef]
34. O'Connor, T.C.; Andzelm, J.; Robbins, M.O. AIREBO-M: A Reactive Model for Hydrocarbons at Extreme Pressures. *J. Chem. Phys.* **2015**, *142*, 024903. [CrossRef]
35. Grantab, R.; Shenoy, V.B.; Ruoff, R.S. Anomalous Strength Characteristics of Tilt Grain Boundaries in Graphene. *Science* **2010**, *330*, 946–948. [CrossRef]
36. Wei, Y.; Wu, J.; Yin, H.; Shi, X.; Yang, R.; Dresselhaus, M. The Nature of Strength Enhancement and Weakening by Pentagong-Heptagon Defects in Graphene. *Nat. Mater.* **2012**, *11*, 759–763. [CrossRef]
37. Huhtala, M.; Krasheninnikov, A.V.; Aittoniemi, J.; Stuart, S.J.; Nordlund, K.; Kaski, K. Improved Mechanical Load Transfer between Shells of Multiwalled Carbon Nanotubes. *Phys. Rev. B* **2004**, *70*, 045404. [CrossRef]
38. Zhu, C.; Liu, X.; Yu, X.; Zhao, N.; Liu, J.; Xu, J. A Small-Angle X-Ray Scattering Study and Molecular Dynamics Simulation of Microvoid Evolution during the Tensile Deformation of Carbon Fibers. *Carbon* **2012**, *50*, 235–243. [CrossRef]
39. Hoover, W.G. Canonical Dynamics: Equilibrium Phase-Space Distributions. *Phys. Rev. A* **1985**, *31*, 1695–1697. [CrossRef]
40. Carbon Fiber. Toray Composite Materials America, Inc. Available online: <https://www.toraycma.com/products/carbon-fiber/> (accessed on 30 July 2021).
41. Tse-Hao, K.; Tzy-Chin, D.; Jeng-An, P.; Ming-Fong, L. The Characterization of PAN-Based Carbon Fibers Developed by Two-Stage Continuous Carbonization. *Carbon* **1993**, *31*, 765–771. [CrossRef]
42. Zhu, C.Z.; Yu, X.L.; Liu, X.F.; Mao, Y.Z.; Liu, R.G.; Zhao, N.; Zhang, X.L.; Xu, J. 2D SAXS/WAXD Analysis of Pan Carbon Fiber Microstructure in Organic/Inorganic Transformation. *Chin. J. Polym. Sci.* **2013**, *31*, 823–832. [CrossRef]

43. Thostenson, E.T.; Li, W.Z.; Wang, D.Z.; Ren, Z.F.; Chou, T.W. Carbon Nanotube/Carbon Fiber Hybrid Multiscale Composites. *J. Appl. Phys.* **2002**, *91*, 6034–6037. [[CrossRef](#)]
44. Yumitori, S.; Arao, Y.; Tanaka, T.; Naito, K.; Tanaka, K.; Katayama, T. Increasing the Interfacial Strength in Carbon Fiber/Polypropylene Composites by Growing CNTs on the Fibers. *Comput. Methods Exp. Meas. XVI* **2013**, *55*, 275–284. [[CrossRef](#)]
45. Zhang, Z.Q.; Ward, D.K.; Xue, Y.; Zhang, H.W.; Horstemeyer, M.F. Interfacial Characteristics of Carbon Nanotube-Polyethylene Composites Using Molecular Dynamics Simulations. *ISRN Mater. Sci.* **2011**, *2011*, 145042. [[CrossRef](#)]